ACCOUNTS
of chemical research

Geometric and Electronic Structure Contributions to Function in Non-heme Iron Enzymes

EDWARD I. SOLOMON,* KENNETH M. LIGHT, LEI V. LIU,
MARTIN SRNEC, AND SHAUN D. WONG

*Department of Chemistry, Stanford University, Stanford,
California 94305-5080, United States*

RECEIVED ON JUNE 28, 2013

CONSPECTUS

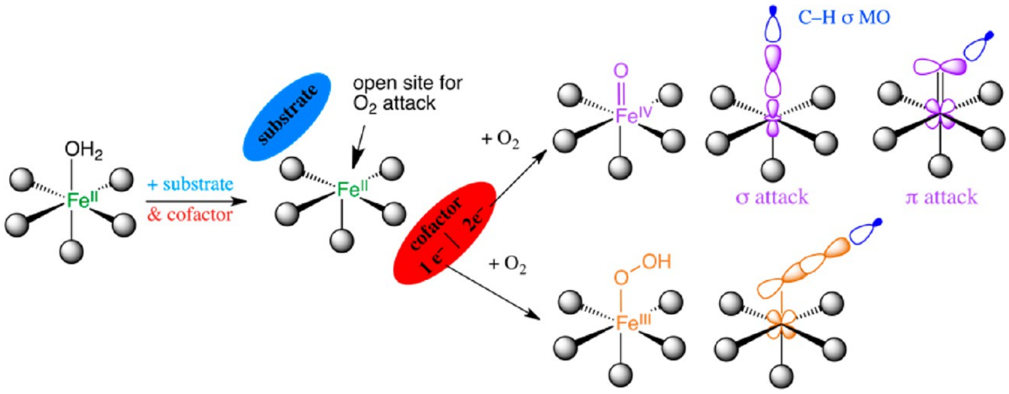

Mononuclear non-heme Fe (NHFe) enzymes play key roles in DNA repair, the biosynthesis of antibiotics, the response to hypoxia, cancer therapy, and many other biological processes. These enzymes catalyze a diverse range of oxidation reactions, including hydroxylation, halogenation, ring closure, desaturation, and electrophilic aromatic substitution (EAS). Most of these enzymes use an Fe^{II} site to activate dioxygen, but traditional spectroscopic methods have not allowed researchers to insightfully probe these ferrous active sites. We have developed a methodology that provides detailed geometric and electronic structure insights into these $NHFe^{II}$ active sites. Using these data, we have defined a general mechanistic strategy that many of these enzymes use: they control O_2 activation (and limit autoxidation and self-hydroxylation) by allowing Fe^{II} coordination unsaturation only in the presence of cosubstrates. Depending on the type of enzyme, O_2 activation either involves a $2e^-$ reduced Fe^{III}−OOH intermediate or a $4e^-$ reduced Fe^{IV}=O intermediate. Nuclear resonance vibrational spectroscopy (NRVS) has provided the geometric structure of these intermediates, and magnetic circular dichroism (MCD) has defined the frontier molecular orbitals (FMOs), the electronic structure that controls reactivity. This Account emphasizes that experimental spectroscopy is critical in evaluating the results of electronic structure calculations. Therefore these data are a key mechanistic bridge between structure and reactivity.

For the Fe^{III}−OOH intermediates, the anticancer drug activated bleomycin (BLM) acts as the non-heme Fe analog of compound 0 in heme (e.g., P450) chemistry. However BLM shows different reactivity: the low-spin (LS) Fe^{III}−OOH can directly abstract a H atom from DNA. The LS and high-spin (HS) Fe^{III}−OOHs have fundamentally different transition states. The LS transition state goes through a hydroxyl radical, but the HS transition state is activated for EAS without O−O cleavage. This activation is important in one class of NHFe enzymes that utilizes a HS Fe^{III}−OOH intermediate in dioxygenation.

For Fe^{IV}=O intermediates, the LS form has a π-type FMO activated for attack perpendicular to the Fe−O bond. However, the HS form (present in the NHFe enzymes) has a π FMO activated perpendicular to the Fe−O bond and a σ FMO positioned along the Fe−O bond. For the NHFe enzymes, the presence of π and σ FMOs enables enzymatic control in determining the type of reactivity: EAS or H-atom extraction for one substrate with different enzymes and halogenation or hydroxylation for one enzyme with different substrates.

www.pubs.acs.org/accounts
10.1021/ar400149m

1. Introduction

Mononuclear non-heme Fe (NHFe) enzymes play key roles in metabolic pathways, hypoxic response, DNA repair, natural product and antibiotic synthesis, and bioremediation.[1,2] Mutations in a number of these enzymes lead to disease states such as phenylketonuria in the case of phenylalanine hydroxylase. The NHFe antibiotic bleomycin (BLM) is a key drug used in treating head, neck, and testicular cancers. At a molecular level, these NHFe sites catalyze a variety of oxidation reactions that include H-atom abstraction for hydroxylation, halogenation, desaturation, or ring closure of a substrate and electrophilic aromatic substitution (EAS) for mono- or dioxygenation. As presented in Table 1, these can be broadly divided into two classes. The lipoxygenases and intradiol dioxygenases use a high-spin (HS) NHFe^{III} center to activate singlet organic substrates for the spin-forbidden reaction with $^3O_2$. However, most NHFe enzymes use a HS NHFe^{II} center to activate O_2. The latter group divides into six subclasses (Table 1A). For the pterin- and α-ketoglutarate (αKG)-dependent enzymes, the cofactor and Fe^{II} each supply two electrons to reduce O_2 to form an $S = 2$ $\text{Fe}^{\text{IV}}{=}\text{O}$ intermediate.[3] For the pterin-dependent family, $\text{Fe}^{\text{IV}}{=}\text{O}$ catalyzes EAS, while in the αKG family, this ferryl intermediate reacts with substrate via H-atom abstraction. For the extradiol dioxygenases two electrons are supplied by the catecholate substrate to reduce O_2 and form a peroxy-quinone-bridged Fe^{II} intermediate.[4] In the Rieske dioxygenases (RDOs), the Fe_2S_2 Rieske center is bridged through a H-bond to the Fe^{II} catalytic site, and together these transfer two electrons to activate O_2 via a high-spin $\text{Fe}^{\text{III}}{-}\text{OOH}$ for *cis*-dioxygenation of an organic substrate.[4] There is also a group of NHFe^{II} enzymes (represented by isopenicillin-N-synthase, IPNS, in Table 1A) that bind non-redox-active substrates and use O_2 for either the two-electron or four-electron oxidation/oxygenation of the substrate. In IPNS, this reaction appears to involve the initial, thermodynamically difficult one-electron reduction of O_2 to form a HS $\text{Fe}^{\text{III}}{—}O_2^{\bullet-}$ intermediate.[5]

TABLE 1. NHFe Enzymes

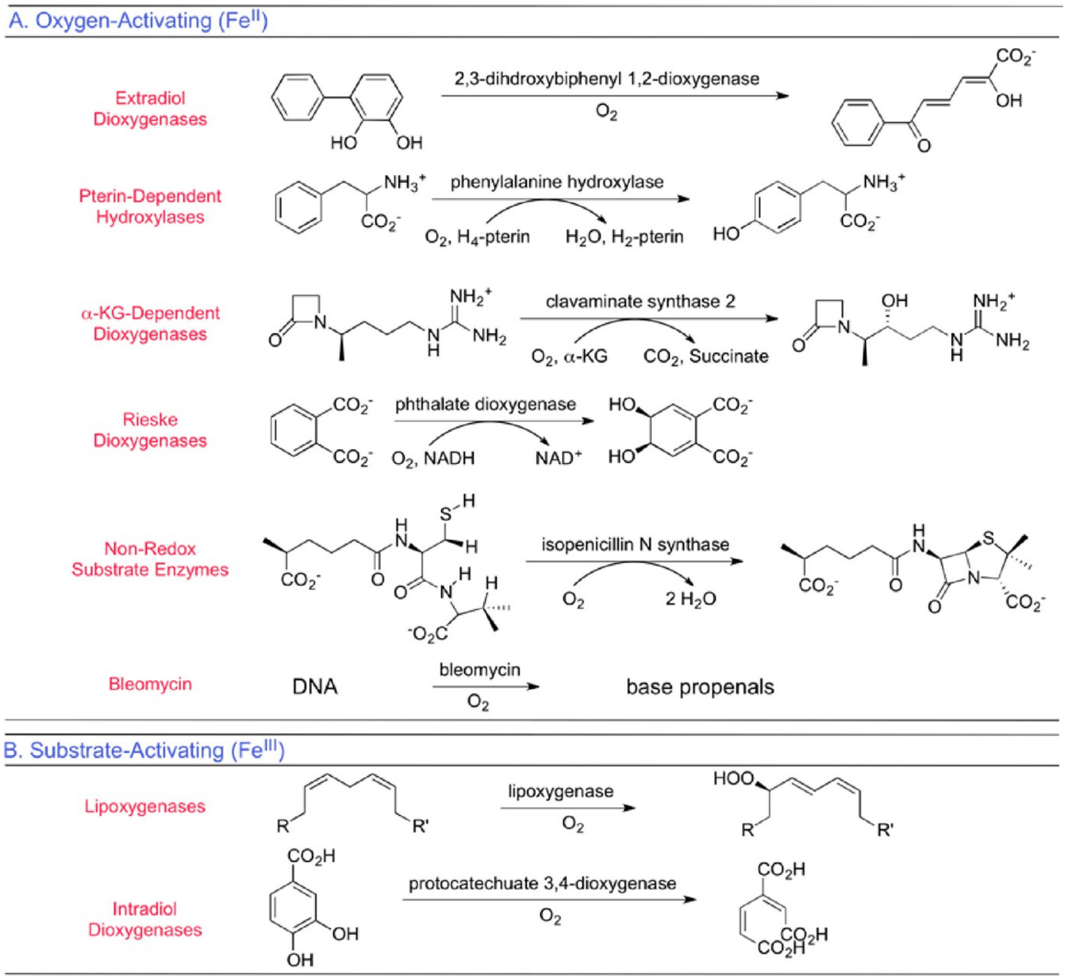

Almost all the NHFe^{II} enzymes utilize a 2-His-1-carboxylate facial triad ligand set of protein residues to bind the Fe^{II}, with additional coordination positions (occupied by waters in the resting enzyme) that are potentially available for O_2, substrate, and cofactor binding. The drug BLM also has a NH ligand set (*vide infra*). BLM uses Fe^{II} to bind O_2 and with one exogenous electron forms activated BLM (ABLM), a low-spin (LS) Fe^{III}−OOH site that abstracts a H-atom from DNA for strand cleavage in its anticancer activity. ABLM is the NHFe analog of compound 0 in P450 heme chemistry (also a LS Fe^{III}−OOH). The latter goes on to protonate and cleave heterolytically to generate compound I (a (Por$^{\bullet-}$)Fe^{IV}═O species[6]) that abstracts a H-atom from strong C−H bonds of substrates.

In this Account, we focus on the NHFe^{II} enzymes and BLM (see ref 7 for a perspective on NHFe^{III} substrate-activating enzymes). We first consider the geometric and electronic structures of the resting Fe^{II} centers and their interactions with substrates that turn on O_2 activation. The NHFe^{II} active site has been challenging to study because the $\pi-\pi^*$ transitions of heme Fe are absent, and these d^6 ions have an $S = 2$ ground state, which is an integer-spin, non-Kramers system where all the spin degeneracy is eliminated by the low-symmetry protein environment and thus produces no EPR signal at X-band. The ferrous active sites in these enzymes have been made accessible through the development of a near-IR (NIR) variable-temperature, variable-field magnetic circular dichroism (VTVH MCD) spectroscopic methodology. This has led to the determination of a general mechanistic strategy used by the NHFe^{II} enzymes in Table 1A. This methodology is surveyed in section 2.1 and used to develop structure/function correlations in section 2.2. For the RDOs and BLM, the O_2 is activated at the hydroperoxo level. In section 3, we consider how the reactivity of the LS Fe^{III}—OOH of the NHFe site in ABLM relates to that of compound 0 in P450 and the activation of HS Fe^{III}—OOH for EAS as in the RDOs. The emphasis here is on the frontier molecular orbitals (FMOs) and how they change with spin. For the αKG- and pterin-dependent NHFe enzymes, the oxygen intermediate key to reactivity is the HS Fe^{IV}═O species. In section 4.1, we use spectroscopy on structurally defined LS and HS Fe^{IV}═O model complexes to experimentally determine the FMOs that are important for reactivity, and in section 4.2, we consider how these FMOs direct H-atom abstraction vs EAS and halogenation vs hydroxylation.

2. Ferrous Active Sites

2.1. NIR VTVH MCD Methodology. From ligand field theory (LFT), an O_h Fe^{II} d^6 HS site has a $^5T_{2g}$ ground state and at an energy 10*Dq* above this is the spin-allowed ^5E_g excited state, where for the N/O facial triad and H_2O ligation $10Dq \approx 10\,000\ \text{cm}^{-1}$.[1] These states are orbitally degenerate and will split in energy in the low-symmetry protein environment. For a six-coordinate (6C) Fe^{II} site, the ^5E_g can split by up to 2000 cm^{-1}. Loss of one ligand to form a five-coordinate (5C) square pyramidal Fe^{II} center leads to a large ^5E splitting, producing LF transitions in the >10 000 and ~5000 cm^{-1} regions. In a 5C trigonal bipyramidal structure, the LF

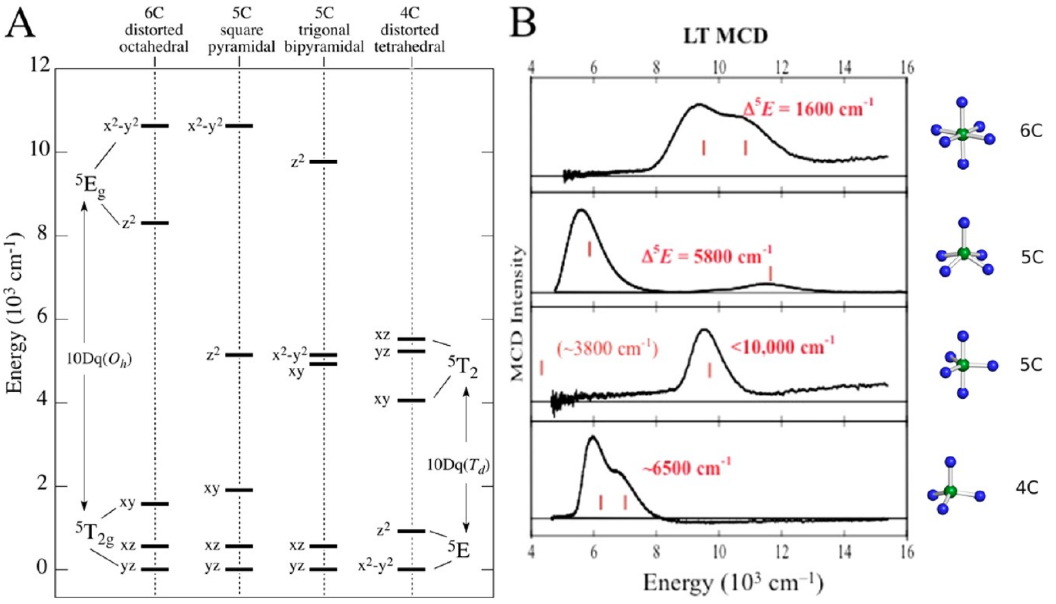

FIGURE 1. NIR MCD transitions for NHFe^{II} sites. (A) Theoretical d orbital splittings for various geometries. (B) Experimentally observed transitions.

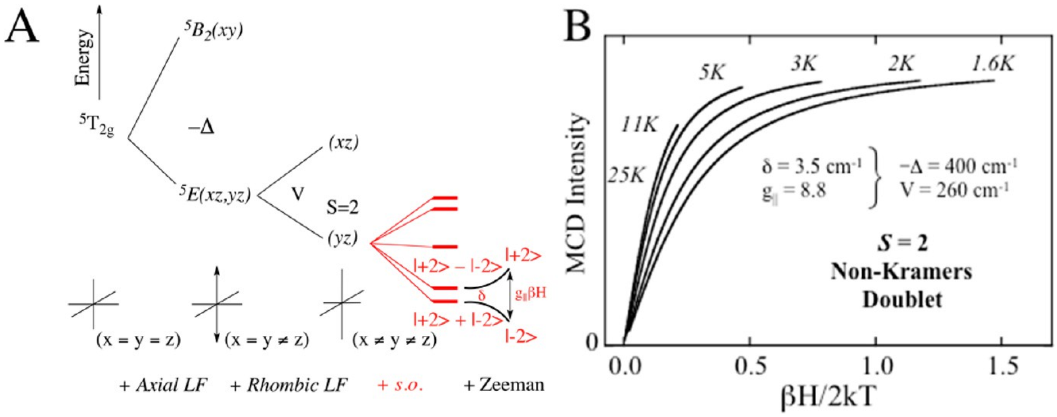

FIGURE 2. VTVH MCD for Fe^{II} sites. (A) Splitting of the $^5T_{2g}$ ground state upon axial and rhombic perturbations. S.O. refers to the effect of spin−orbit coupling. (B) Nested MCD isotherms for an $S = 2$ non-Kramers doublet.

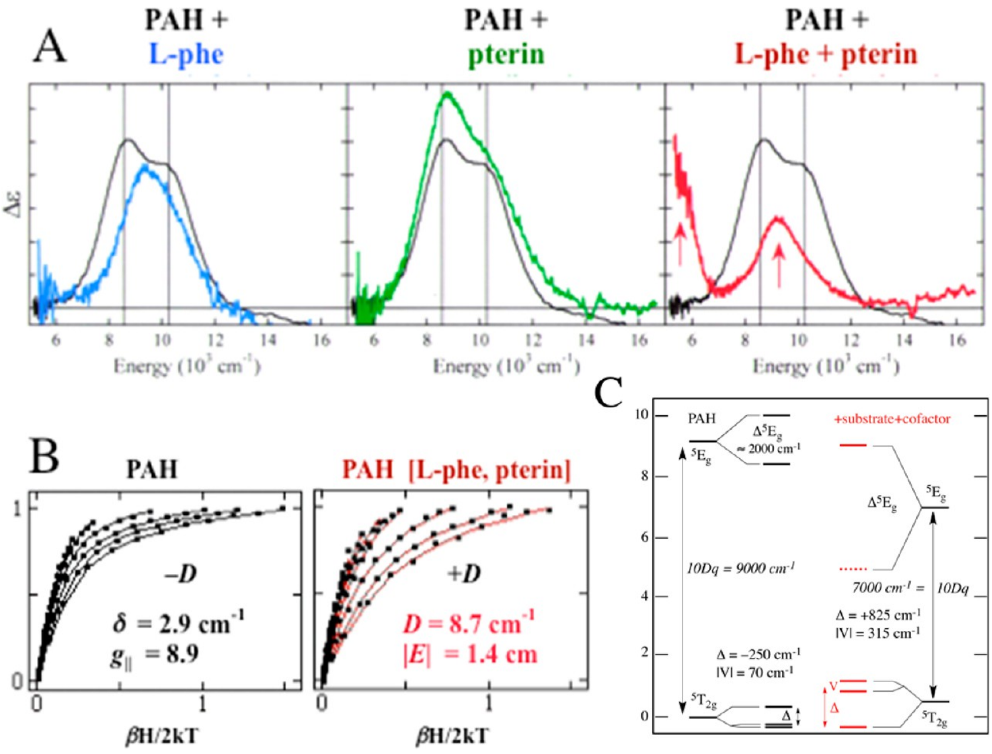

FIGURE 3. MCD studies of PAH. (A) MCD spectra of resting PAH (black) with substrate bound (blue), pterin bound (green), and substrate and pterin bound (red). All spectra were collected at 5 K. (B) VTVH MCD data for resting (left) and substrate and pterin bound (right) PAH. (C) Derived d-orbital energy level diagrams. Adapted from Reference 8.

changes and the transitions shift to <10 000 and <5000 cm^{-1}, and in a 4C distorted tetrahedral site, since 10*Dq* (T_d) = −4/9(10*Dq*) (O_h), there are only LF transitions in the ∼5000−7000 cm^{-1} region. Thus from Figure 1A, the energy splittings of the d orbitals and associated d → d transitions are very sensitive to the LF of the Fe^{II} site.

Since d → d transitions are parity-forbidden, they are weak in absorption (abs.), and since these are in the NIR spectral region where intense vibrations from the protein and buffer contribute, these cannot be studied by abs. spectroscopy. However, since the ground state is $S = 2$, the sites can be directly studied by NIR MCD at low temperature (LT) where the "*C*-term" MCD signals of paramagnetic centers are orders of magnitude larger than those of the diamagnetic background. The LT MCD spectra of >20 structurally defined Fe^{II} complexes with different coordination environments have been studied and found to be as predicted by LFT as shown in Figure 1B.[1]

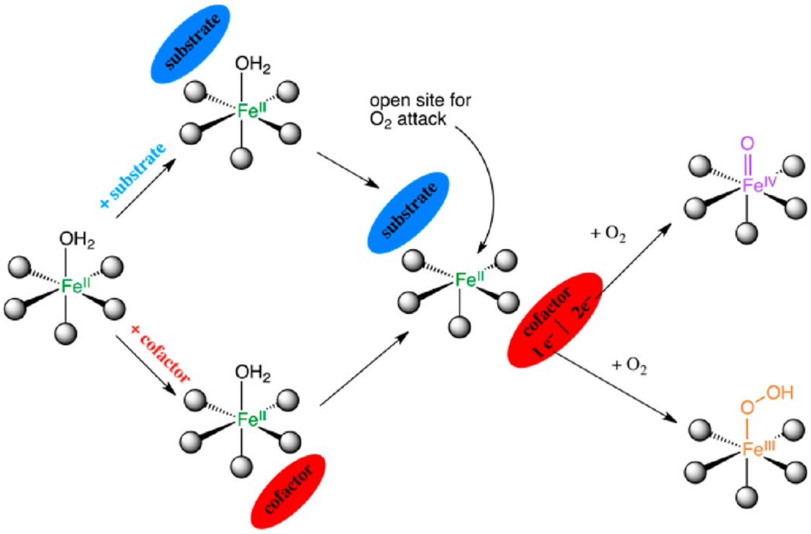

FIGURE 4. General mechanistic strategy for O_2 activation by $NHFe^{II}$ enzymes.

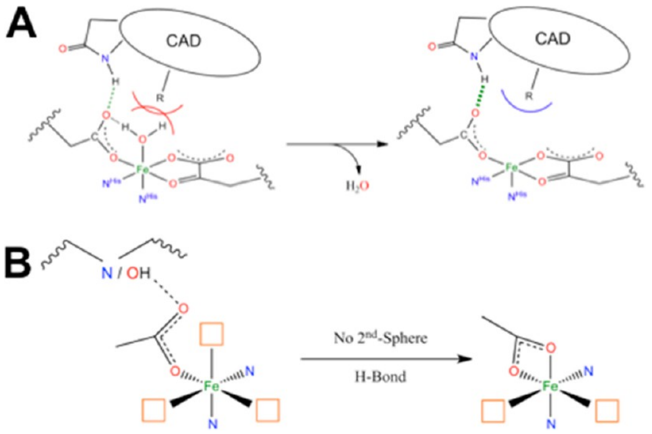

FIGURE 5. (A) Steric and H-bonding contributions to loss of coordinated H_2O. CAD stands for C-terminal activation domain of the substrate HIF-1α. (B) Effect of a second-sphere H-bonding partner on the facial triad carboxylate.

From Figure 2A, the 3-fold-degenerate $^5T_2$ ground state also splits in energy in the low-symmetry protein environment, reflecting differences in dπ interactions with the ligands. This can be studied directly by VTVH MCD.[1] A HS Fe^{II} center will produce a set of nested saturation magnetization curves as shown in Figure 2B. This nesting is due to the nonlinear energy splitting and mixing of the M_S sublevels of the $S = 2$ ground state, and fitting these data gives the ground-state splitting (δ, $g_{\parallel}$) that in turn is determined by the axial (Δ) and rhombic (V) splittings of the dπ orbitals. Thus for the $NHFe^{II}$ sites, we are able to *experimentally* determine the energies of the five d orbitals (Figure 1A), which reflect the active site geometric and electronic structure.

2.2. General Mechanistic Strategy. The above methodology has been applied to define structure/function

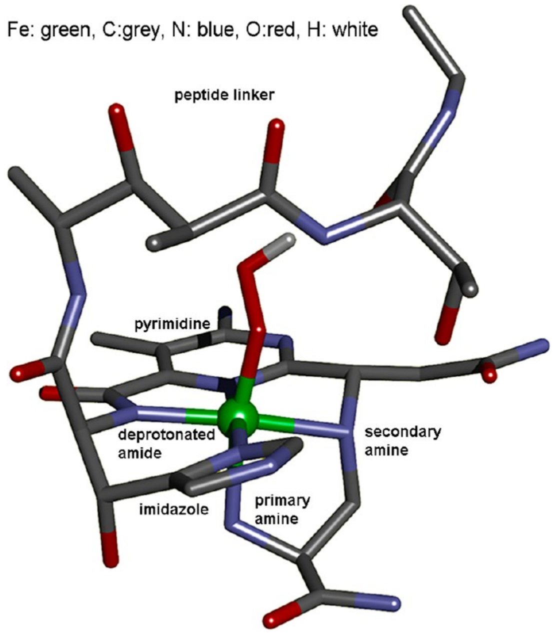

FIGURE 6. Optimized structure of ABLM.

correlations over a number of $NHFe^{II}$ enzymes in each of the subclasses in Table 1A. The data presented in Figure 3 on the pterin-dependent enzyme phenylalanine hydroxylase (PAH) (with Caradonna et al.[8]) are representative of the behavior we observe for all three pterin-dependent enzymes and in general for all the subclasses of $NHFe^{II}$ enzymes. Resting PAH exhibits the LT MCD spectrum in black, showing two LF transitions in the ~10 000 cm^{-1} region split by ~2000 cm^{-1}. Thus the resting Fe^{II} site is 6C. Upon addition of phenylalanine substrate, the blue spectrum is obtained, showing a slightly perturbed 6C Fe^{II} site.

Addition of pterin to the resting Fe^{II} enzyme produces the green LT MCD spectrum showing that the pterin cofactor does not bind to the Fe^{II}. Importantly when both pterin and substrate are added to resting PAH, the LT MCD spectrum in red is obtained with one LF transition at ~10 000 cm^{-1} and one in the ~5000 cm^{-1} region. Also, the VTVH MCD saturation magnetization curves change dramatically upon substrate-plus-cofactor binding to resting Fe^{II} PAH (Figure 3B). These data give the experimental LF splittings of the five d orbitals in Figure 3C. In the resting, substrate-bound and only-cofactor-bound Fe^{II} forms, 10*Dq* is large and there is only a limited splitting of E and T_2 orbital degeneracies, reflecting 6C sites. Alternatively when both substrate and cofactor are bound to the enzyme, 10*Dq* greatly decreases and there is a large splitting of E and T_2 degeneracies, all showing that the Fe^{II} active site becomes 5C upon binding both cosubstrates.

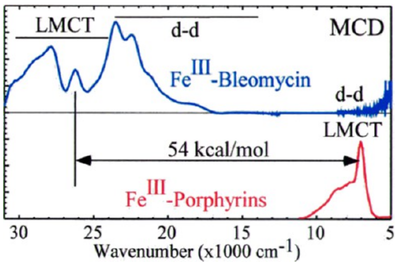

FIGURE 7. MCD spectral comparison of LMCT energies of $(BLM)Fe^{III}$ (deprotonated amide to Fe^{III}) and a prototypical Fe^{III}-heme (porphyrin to Fe^{III}). Adapted from Reference 12.

Parallel NIR VTVH MCD studies have been performed over a range of other $NHFe^{II}$ enzymes, which have led to the general mechanistic strategy used by this class of enzymes shown in Figure 4. The resting Fe^{II} state and sites with either substrate or cofactor bound are 6C and relatively stable to reaction with O_2, which at this stage would lead to uncoupled turnover and potentially self-hydroxylation. However, when both the substrate and the cofactor are bound to the enzyme, the Fe^{II} site becomes 5C, with an open coordination position for O_2 activation.

This 6C → 5C conversion involves the loss of a H_2O ligand. The molecular basis for the substrate-induced H_2O loss has been defined (in collaboration with Knapp et al.[9]) in FIH (involved in hypoxic signaling) and has been found to involve both steric clashes between H_2O and substrate in the 6C form and stabilization of the 5C form through H-bonding to the facial triad carboxylate (Figure 5A).

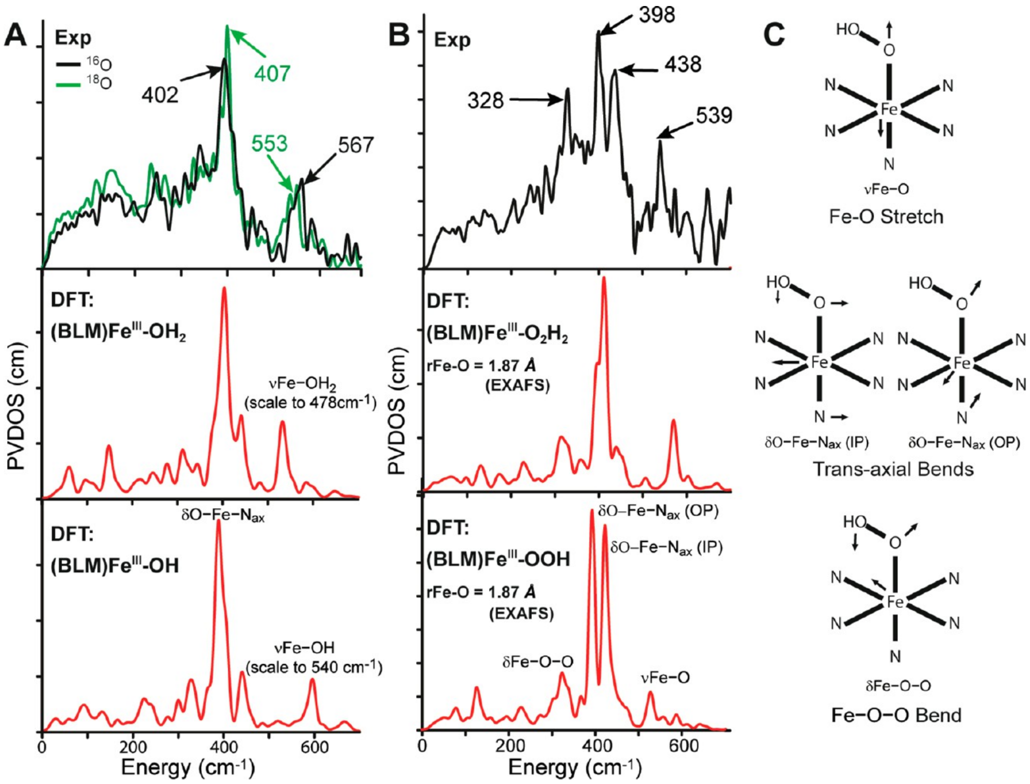

FIGURE 8. (A) NRVS spectra (PVDOS) of ^{16}O and ^{18}O $(BLM)Fe^{III}$ (top) and DFT-simulated PVDOS spectra of two models with H_2O (middle) and OH^- (bottom) as axial ligands. (B) NRVS spectrum of ABLM (top) and DFT-simulated spectra with H_2O_2 (middle) and OOH^- (bottom) as axial ligands. (C) Major NRVS-active vibrational modes of ABLM. Adapted from Reference 10.

With respect to the facialtriad carboxylate, there are interesting differences among the different subclasses that reflect second-sphere interactions that are important for O_2 reactivity. For the αKG-dependent and extradiol enzymes, the cofactor/cosubstrate binds bidentate to Fe^{II}. Because O_2 must also bind to Fe^{II} for catalysis, three coordination sites are needed for reactivity (Figure 5B, left). However, for a 5C Fe^{II} site, the facialtriad carboxylate will switch to bidentate coordination (Figure 5B, right), which would prevent catalysis.[9] Extradiol dioxygenases and αKG-dependent enzymes avoid this by having a second-sphere residue available to H-bond to the facialtriad carboxylate. For the pterin-dependent and RDO enzymes, neither substrate nor cofactor binds to the Fe^{II}. Members of these subclasses do not have a second-sphere residue H-bond to the facial triad carboxylate; thus it coordinates to the Fe^{II} in a bidentate mode, allowing O_2 to bind in a single orientation for proper reactivity (Figure 5B, right). For pterin-dependent enzymes, O_2 must bind in an end-on fashion for bridging between Fe^{II} and the pterin cofactor, cleave, and rearrange for reaction with substrate. For Rieske dioxygenases, a side-on bidentate binding mode for O_2 is required for formation of the reactive intermediate.

3. Fe^{III}−Hydroperoxy Intermediates

Fe^{III}−OOH intermediates are important in ABLM, which is LS ($S = 1/2$), and in the RDOs, which are HS ($S = 5/2$). ABLM is the NHFe intermediate closest to that in heme chemistry, and in section 3.1, we contrast their reactivity. In section 3.2, we evaluate how spin state influences the FMOs and affects the transition state (TS) and its relation to function in the RDOs.

TABLE 2. Thermodynamics of Heterolytic Cleavage of O−O Bonds in P450 and ABLM and Direct H-Atom Abstraction by ABLM

	thermodynamics (kcal/mol)			
reactant	ΔE	ΔE(solv)	$-T\Delta S$	ΔG
$Fe^{III}(Por)(SCH_3)$−OOH heterolytic	−75	−52	−6	−58
Fe^{III}(BLM)−OOH heterolytic	+99	+20	−7	+13
Fe^{III}(BLM)−OOH direct H-atom	+13	+9	−16	−7

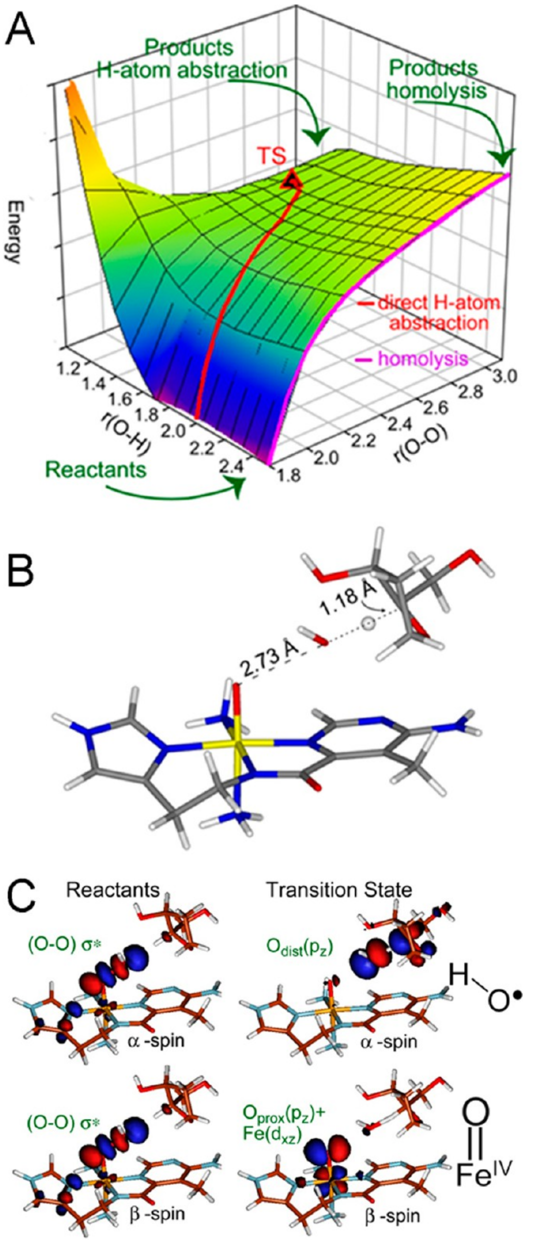

FIGURE 9. (A) PES for H-atom abstraction by ABLM. (B) TS of direct H-atom abstraction. (C) FMOs of ABLM before (left) and at the TS (right). Adapted from Reference 15.

3.1. Low-Spin Non-Heme vs Heme. (BLM)Fe^{II} binds O_2 and takes up an exogenous e^- to form ABLM, a LS ferric-hydroperoxide (Figure 6).[10] ABLM is the intermediate before H-atom abstraction from the C4′ position of DNA.[11] In the heme analog, compound 0 of P450, this LS Fe^{III}−OOH protonates and heterolytically cleaves to form compound I, an Fe^{IV}=O porphyrin radical, that abstracts a H-atom from strong H−C bonds. There has been significant interest in whether ABLM parallels heme chemistry to generate an unobserved compound I analog that does the DNA cleavage. Thus, we used calculations supported by the spectroscopic data to elucidate the relative energies of the protonation/heterolytic cleavage reactions in ABLM and compound 0 in P450. From Table 2, this reaction is calculated to be 71 kcal/mol less favorable in ABLM relative to P450 and endergonic by 13 kcal/mol.[12] This reflects the fact that delocalization of the hole over the π system of the porphyrin and its −2 charge facilitate ligand oxidation in heme relative to a non-heme ligand set, as evidenced by the much-higher-energy of the lignd-to-metal charge transfer

(LMCT) transitions of (BLM)Fe^{III} as compared with heme (Figure 7).

These considerations lead to the alternative hypothesis of direct H-atom abstraction from the substrate by ABLM.[12] From the calculations listed in Table 2, this reaction is 20 kcal/mol more favorable than the heterolytic cleavage reaction and exergonic by 7 kcal/mol.

However, a computational study considering the peroxo-shunt reaction argued for a (BLM)Fe^{III}—H_2O → (BLM)Fe^{III}—H_2O_2 conversion, and the presence of the additional proton would make the heterolytic cleavage more favorable by 15 kcal/mol, comparable to direct H-atom abstraction by (BLM)$Fe^{III}-OOH$.[13]

Thus it was necessary to experimentally determine the nature of the axial ligands in (BLM)Fe^{III} and ABLM. Since ABLM is unstable in a laser, we turned to nuclear resonance vibrational spectroscopy (NRVS). From Figure 8, the spectrum for (BLM)Fe^{III} shows a $H_2{}^{18}O$ isotope-sensitive vibration at 567 cm^{-1}, which combined with an EXAFS distance of 1.86 Å and computational modeling (Figure 8A, bottom) assigns the axial ligand as hydroxide.[10] It also exhibits a dominant feature at 407 cm^{-1}, which reflects the degenerate pair of *trans*-axial bends (Figure 8C) that has dominant Fe motion. In going to the NRVS spectrum of ABLM, this pair splits into two peaks at 438 and 398 cm^{-1}, and an additional feature is present at 328 cm^{-1}. This *trans*-axial splitting is only reproduced by the $Fe^{III}-OOH$ structure of ABLM where the 328 cm^{-1} peak is the Fe−O−O bend, and this mixes with the in-plane *trans*-axial bend leading to the peak splitting.

ABLM is confirmed to be a LS $Fe^{III}-OOH$ species; thus its protonation and heterolytic cleavage to produce a heme-type compound I is unfavorable by 20 kcal/mol relative to its direct H-atom abstraction from DNA, Table 2. The direct reaction of ABLM requires that DNA participate in the TS. DNA does in fact accelerate this reaction by ~2.5 times and changes ABLM's decay kinetics from having a relatively small primary KIE (3.6 ± 0.9, from self-decay) to a large secondary KIE with DNA (1.7 ± 0.2, nonexchangeable H−C4′ group).[14]

These experimental data were modeled with a 2D potential energy surface (PES) for the H-atom abstraction from the H−C bond of a substrate by ABLM (Figure 9A).[15] A TS was found that reproduces experiment with an E_a of 13 kcal/mol, about half that calculated for heterolytic cleavage and H-atom abstraction. The TS for direct $Fe^{III}-OOH$ attack on DNA also reproduces the small primary and large secondary KIEs that reflect a TS that is late in O−O cleavage but early in H-atom abstraction (Figure 9B).

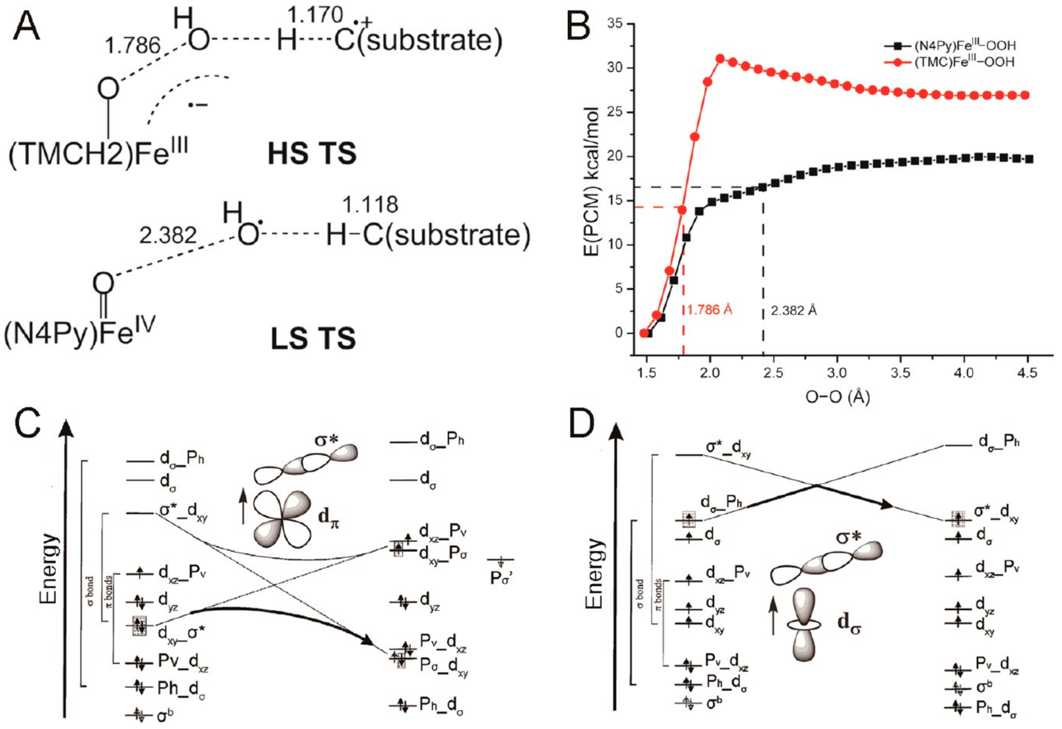

FIGURE 10. (A) TSs of HS (TMC)$Fe^{III}-OOH$ and LS (N4Py)$Fe^{III}-OOH$ in H-atom abstraction. (B) PESs of HS (TMC)$Fe^{III}-OOH$ and LS (N4Py)$Fe^{III}-OOH$ O−O homolysis. Calculations were performed using the polarizable continuum model (PCM) with a dielectric constant of acetone. (C, D) Forbidden and allowed orbital crossings for O−O bond homolysis of LS and HS Fe^{III}−alkylperoxo complexes. See ref 17 for details. Adapted from Reference 16.

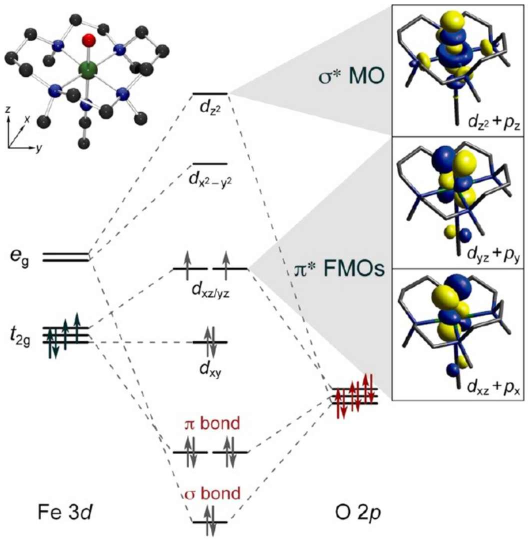

FIGURE 11. MO diagram for $S = 1$ (TMC)$Fe^{IV}{=}O$ (inset, top left) producing π^* FMOs and σ^* MO (right). Adapted from Reference 20.

This relates to the FMO of the LS $Fe^{III}-OOH$, which is the lowest-unoccupied hydroperoxide σ^* orbital. From Figure 9C, elongation of the O−O to the TS greatly weakens the peroxo σ/σ^* interaction and allows its α- and β-spin holes to polarize: one on the distal O making this a $OH^\bullet$ radical that is efficient in H-atom abstraction, and the other localizes on the proximal O generating an $Fe^{IV}{=}O$ species. The latter is effective in performing a second H-atom abstraction from DNA, leading to double-strand cleavage important for BLM's anticancer activity.

3.2. Low-Spin to High-Spin $Fe^{III}-OOH$ FMOs. In going to the RDOs, the $Fe^{III}-OOH$ intermediate is HS.[4] Spectroscopic studies were performed (with Nam and co-workers[16]) on $S = 1/2$ (N4Py)$Fe^{III}-OOH$ and the $S = 5/2$ (TMC)$Fe^{III}-OOH$ models and correlated to electronic structure calculations to understand differences in their reactivities. For LS $Fe^{III}-OOH$, the TS

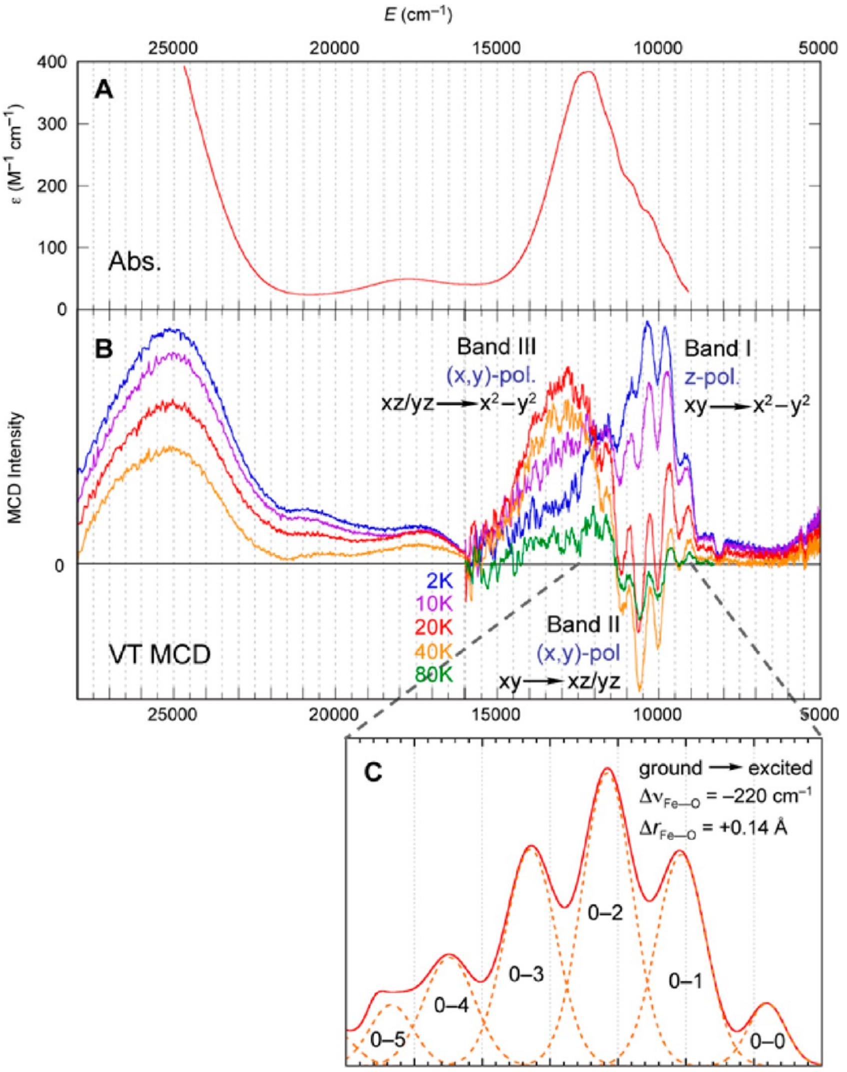

FIGURE 12. (A) The 233 K abs. and (B) VT MCD spectra of (TMC)$Fe^{IV}{=}O$. (C) Vibronic progression of band II (40 K; plotted positive). Adapted from Reference 20.

for H-atom abstraction is *again* late in O–O cleavage, generating a OH$^•$ for H-atom abstraction.

In contrast, in the HS[16] Fe^{III}–OOH complex, the TS is early in O–O cleavage and later in H-atom abstraction, Figure 10A. The origin of this difference in TSs is the spin-state dependence of O–O bond homolysis (Figure 10B), where the HS Fe^{III}–OOH has an additional 12 kcal/mol barrier. This derives from the different interactions between redox-active orbitals in LS and HS Fe^{III}–OOH (Figure 10, panel C vs D).[17]

The relatively low barrier for O–O homolysis in the LS system allows generation of a OH$^•$ for H-atom abstraction. Alternatively for the HS Fe^{III}–OOH complex, the larger barrier for homolysis leads to a relatively short O–O bond (1.79 Å) at the TS for H-atom abstraction (Figure 10A). At this TS, significant electron density is transferred from the substrate into the Fe^{III}–OOH LUMO due to the higher reduction potential of the HS complex. This leads to an important spin-state dependence of the reaction barrier on the substrate. LS Fe^{III}–OOH (e.g., ABLM) is favored for H-atom abstraction from strong H–C bonds, while HS Fe^{III}–OOH is activated for electrophilic attack on substrates without O–O bond cleavage. The latter is important for the RDOs where both oxygen atoms of the hydroperoxide are inserted into *cis* positions of aromatic substrates.

4. Fe^{IV}=O Intermediates

For the αKG and pterin-dependent enzymes, the cofactor and Fe^{II} each donate 2e$^-$ to dioxygen to generate $S = 2$ Fe^{IV}=O intermediates. The pterin-dependent enzymes perform electrophilic aromatic substitution (EAS); the αKG-dependent enzymes abstract an H-atom, followed by rebound hydroxylation for the facialtriad enzymes or halogenation in the halogenases where the facialtriad carboxylate is replaced by a halide. In section 4.1, we consider the FMOs available for these reactivities in structurally defined $S = 1$ and $S = 2$ Fe^{IV}=O model complexes.[18,19] In section 4.2, we extend these FMO concepts to understand the factors that control EAS vs H-atom abstraction and for the latter the factors that control hydroxylation vs halogenation.

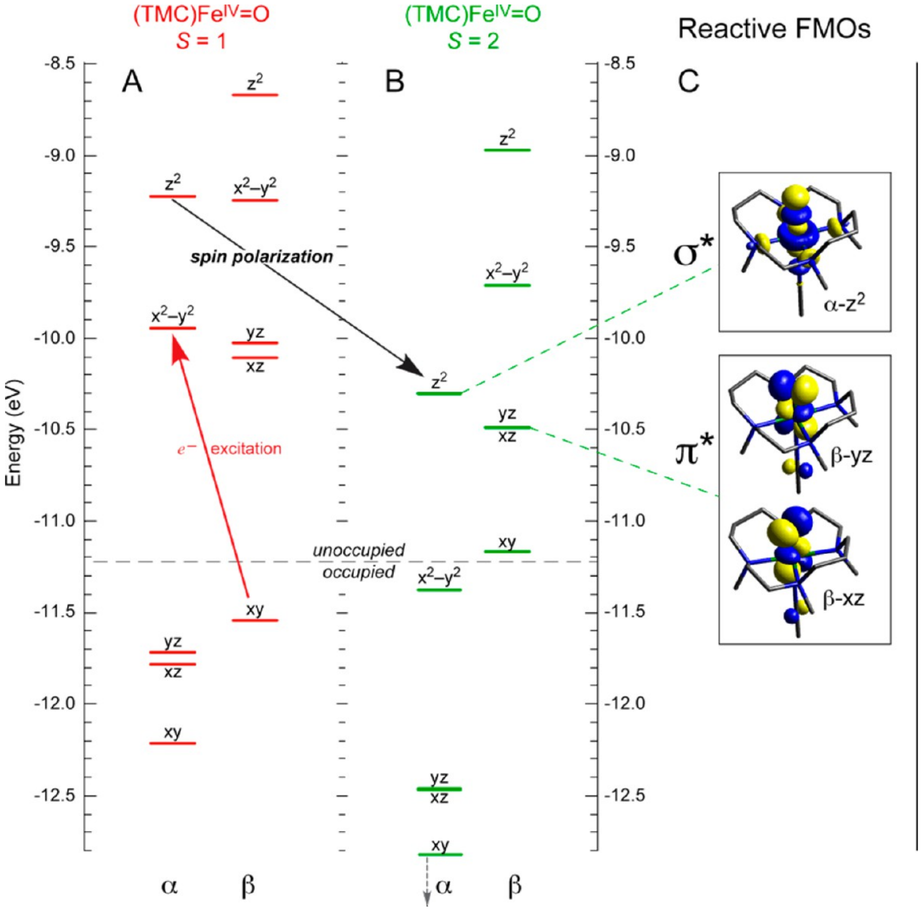

FIGURE 13. MO diagrams of (TMC)Fe^{IV}=O in (A) $S = 1$ (ground) and (B) $S = 2$ states, showing that excitation of β-d$_{xy}$ e$^-$ into α-d$_{x^2-y^2}$ orbital leads to spin polarization of the α-manifold and a low-energy α-d$_{z^2}$ FMO for reactivity. (C) Isosurface plots of $S = 2$ FMOs.

4.1. FMOs. The bonding description of the first structurally defined $S = 1$ $\mathrm{Fe^{IV}{=}O}$ model complex, $\mathrm{(TMC)Fe^{IV}{=}O}$,[18] is shown in Figure 11: at high energy is the d_{z^2} orbital, which is strongly σ antibonding with the oxo p_z, and at lower energy is the Fe $\pi^*{-}d_{xz,yz} -$ oxo $p_{x,y}$ combination, forming the $d\pi^*$ β FMOs available for reactivity. These FMOs were studied directly (with Que et al.[20]) by using abs. and MCD spectroscopies to probe the $d_{xy}(nb) \rightarrow d_{xz,yz}(\pi^*)$ excitation. The weak, relatively uninformative abs. band at $\sim$12 000 $\mathrm{cm^{-1}}$ (Figure 12A) results from three overlapping transitions as revealed by VT MCD (Figure 12B). These three transitions have different temperature-dependent MCD behaviors that reflect the different polarizations of the electronic transitions. Importantly, overlapping band I is the negative, sharp band II, the lowest-energy (x,y)-polarized $d_{xy} \rightarrow d_{xz,yz}$ LF transition. Band II directly experimentally probes the $d\pi^*$ FMO of this $\mathrm{Fe^{IV}{=}O}$ complex and shows (from the associated vibrational progression, Figure 12C) a strong π-antibonding interaction, which shifts significant O $p\pi$ character into the $d\pi^*$ orbitals, activating them for electrophilic attack perpendicular to the Fe−O bond.[20]

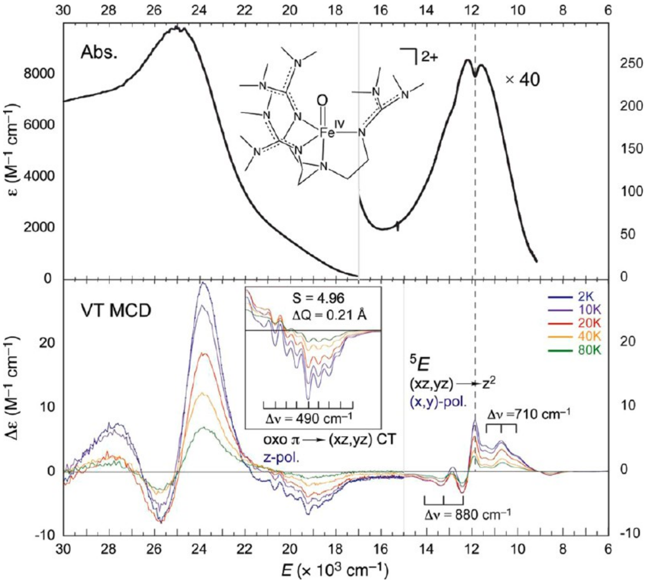

FIGURE 14. The 233 K Abs. (top) and VT MCD (7 T, bottom) spectra of $\mathrm{(TMG_3tren)Fe^{IV}{=}O}$ showing structured features corresponding to FMOs. Adapted from Reference 21.

In going from an $S = 1$ to an $S = 2$ ground state of $\mathrm{Fe^{IV}{=}O}$, a β e^- in d_{xy} is transferred into the $d_{x^2-y^2}$ orbital. This does not affect the $\mathrm{Fe^{IV}{=}O}$ bond; however, there is a significant effect on the low-lying unoccupied FMOs. From the spin-unrestricted MO diagram in Figure 13, excitation of a β e^- from the d_{xy} into the α-$d_{x^2-y^2}$ orbital leads to stabilization of the α-spin manifold due to the spin polarization associated with differences in exchange. This brings the α-d_{z^2} σ^* orbital down to an energy comparable to the $d\pi^*$ FMO. However, the d_{z^2} σ^* has oxo p_z character oriented along the Fe−O bond (Figure 13C). Thus, for the $S = 2$ $\mathrm{NHFe^{IV}{=}O}$ intermediates, there are two low-lying unoccupied FMOs available for H-atom abstraction and EAS: the $d\pi^*$ FMO with oxo $p_{x,y}$ character perpendicular to the Fe−O bond and the $d\sigma^*$ FMO with oxo p_z character for attack along the Fe−O bond.

Studies on the first structurally defined $S = 2$ $\mathrm{Fe^{IV}{=}O}$ complex $\mathrm{(TMG_3tren)Fe^{IV}{=}O}$[19] (with Que et al.[21]) revealed relatively uninformative low-energy weak and high-energy intense abs. bands but high-information-content LT MCD spectra (Figure 14). The band at $\sim$12 000 $\mathrm{cm^{-1}}$ is assigned as the lowest-energy ${}^5A \rightarrow {}^5E$ $(d_{xz,yz} \rightarrow d_{z^2})$ LF transition, based

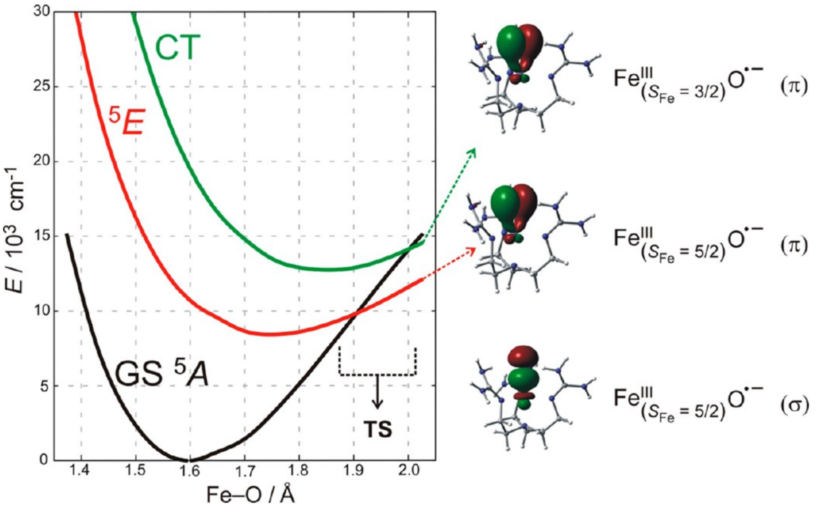

FIGURE 15. (left) PES of $S = 2$ states along the Fe−O coordinate for $\mathrm{(TMG_3tren)Fe^{IV}{=}O}$, which lead to one σ and two π FMOs of $\mathrm{Fe^{III}}$—oxyl character (right) at the TS. Adapted from Reference 21.

on its pseudo-*A* (derivative) shape and temperature-dependent behavior. Interestingly, the sharp positive peak overlapping this band corresponds to a dip in abs. (dashed line), indicating a Fano antiresonance of this allowed ^5E state with a spin-forbidden ^3A. Furthermore, the two different vibronic progressions associated with this ^5E indicate strong spin–orbit coupling (SOC) with another nearby triplet (^3E), which distorts the ^5E PES. Also, from the MCD spectra, the low-energy shoulder in the abs. spectrum at ~20 000 cm^{-1} corresponds to a pronounced, negatively signed *z*-polarized (i.e., Fe–O) vibronic progression with a ν_{Fe-O} of 490 cm^{-1}, greatly reduced from that of the ground state (~830 cm^{-1}). These excited-state properties led to the assignment of this band as the oxo $\pi \rightarrow d_{xz,yz}$ CT transition. Thus, spectroscopy on (TMG$_3$tren)Fe^{IV}=O reveals three FMOs: the d_{z^2} σ^* ground state, the low-lying dπ^* and a higher-energy oxo πFMO.[21]

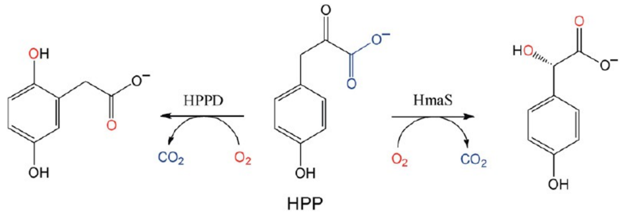

FIGURE 16. Reactions of HPP with HPPD (left, EAS) and HmaS (right, H-atom abstraction) to produce homogentisate and (4-hydroxy)-mandelate, respectively.

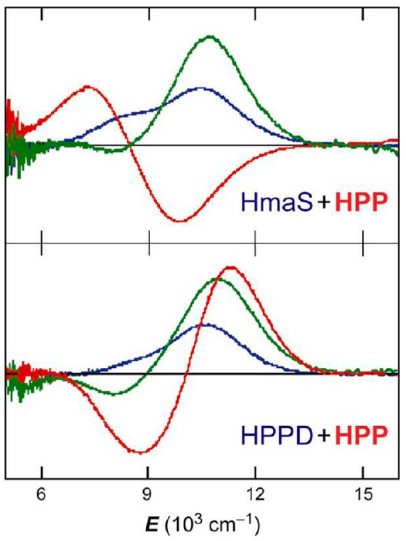

FIGURE 17. CD spectra of HPP binding (red lines) to HmaS (top) and HPPD (bottom) Fe^{II} sites. Resting Fe^{II} d–d transitions (blue), and pyruvate-bound-Fe^{II} (green) as controls. Adapted from Reference 22.

CASPT2 calculations reproducing these spectral features (Figure 15) were extrapolated to the Fe–O bond length associated with the TS for H-atom abstraction.[21] These low-lying states generate (Figure 15, right) three comparable (in energy and coefficients on the oxo) FMOs, one σ and two π, with the former oriented for attack along the Fe–O bond and the latter two oriented for perpendicular attack on substrates. Importantly, all three FMOs polarize at the TS, generating Fe^{III}—oxyl species with high oxygen p hole character for effective electrophilic reactivity.

Thus, spectroscopy correlated to electronic structure calculations has revealed that in contrast to Fe^{IV}=O $S = 1$ species where only a π-FMO is available for electrophilic reactivity perpendicular to the Fe^{IV}=O bond, Fe^{IV}=O $S = 2$ intermediates have both σ and π-FMOs available for reactivity, respectively, along and perpendicular to the Fe^{IV}=O bond.

4.2. Structure/Function Correlations.

4.2.1. H-Atom Abstraction vs Electrophilic Aromatic Substitution. (4-Hydroxyphenyl)pyruvate dioxygenase (HPPD) and (4-hydroxy)-mandelate synthase (HmaS) both react with the same substrate, (4-hydroxyphenyl)pyruvate (HPP); HPPD performs EAS on the ring, while HmaS performs H-atom abstraction (Figure 16). HPP has an α-keto acid group that binds in a bidentate mode that directly tethers this substrate to the Fe^{II}. From the CD data (with Moran and Spencer et al.[22]) in Figure 17, HPP is bound to the two Fe^{II} enzymes with different conformations of the ring, consistent with their different reaction products (Figure 16). The O$_2$ reaction[22] produces the two Fe^{IV}=O intermediates

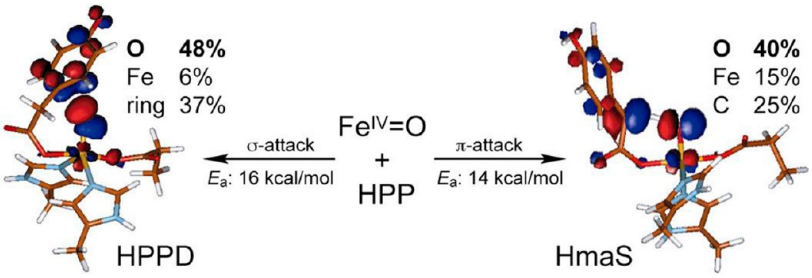

FIGURE 18. Reactivities of Fe^{IV}=O intermediates in HPPD (left) and HmaS (right), with different substrate (HPP) conformations leading to a σ TS for EAS in HPPD and a π TS for H-atom abstraction in HmaS. Formation of Fe^{III}—O$^{\bullet-}$ species at TS provides FMOs primed for reactivity. Adapted from Reference 22.

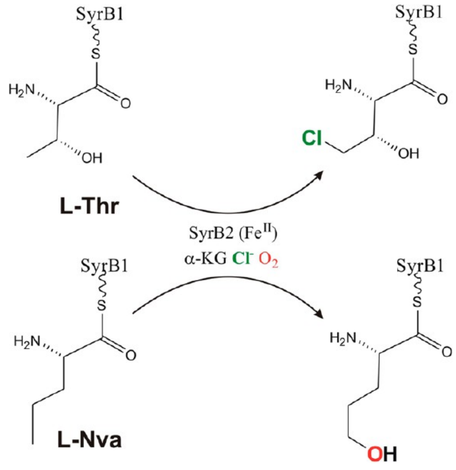

FIGURE 19. SyrB2 catalyzes both chlorination of native substrate L-Thr (top) and hydroxylation of alternative substrate L-Nva (bottom).

(Figure 18). For HPPD, the Fe–O bond is oriented for σ electrophilic attack on the aromatic ring, while in HmaS, the Fe–O bond is oriented perpendicular to the H–C bond of the substrate and activated for π H-atom abstraction. For both reaction coordinates, the Fe–O bond elongates and polarizes at the TS to become $Fe^{III}–O^{\bullet-}$. This provides low-lying unoccupied oxo $p\sigma$ (for HPPD) and $p\pi$ (for HmaS) FMOs, leading to comparable low-energy barriers for EAS (16 kcal/mol, HPPD) and H-atom abstraction (14 kcal/mol, HmaS).[22]

4.2.2. Halogenation vs Hydroxylation. For the halogenases, which include SyrB2, which catalyzes the chlorination of L-Thr in syringomycin E biosynthesis, the carboxylate ligand of the Fe^{II} facial triad is replaced by a halide (Cl^-/Br^-).[3] These halogenases bind αKG and react with O_2 to generate an $Fe^{IV}{=}O$ intermediate[3] that abstracts a H-atom and in the case of SyrB2 with its native substrate rebounds to form the halogenated product 4-Cl-L-Thr (Figure 19, top). With the alternative substrate L-Nva (Figure 19, bottom), the $Fe^{IV}{=}O$ intermediate abstracts a H-atom but rebounds to produce a hydroxylated product.[23] Thus, in complement to the studies described in section 4.2.1 where two NHFe enzymes perform different reactions with the same substrate (HPP), for the halogenases one NHFe enzyme performs different reactions depending on substrate.

In collaboration with Bollinger and Krebs et al.,[24] the first NRVS spectra of any oxygen intermediate were obtained. This $Fe^{IV}{=}O$ intermediate can be generated with either Cl^- or Br^- bound to the NHFe active site, providing an important mass perturbation on the NRVS data. The data in Figure 20 show that the $Fe^{IV}{=}O$ intermediate has three dominant peaks in its NRVS spectrum at around 370, 300, and 250 cm^{-1}, and the intensity shifts from the higher-energy peaks in the Cl cognate into the lowest-energy peak in the Br cognate. These NRVS spectra and their Cl → Br perturbation are only reproduced with a 5C TBP structure with the $Fe^{IV}{=}O$ bond defining the trigonal axis (Figure 20, bottom). This is the first direct structural insight into any $NHFe^{IV}{=}O$ intermediate.[24]

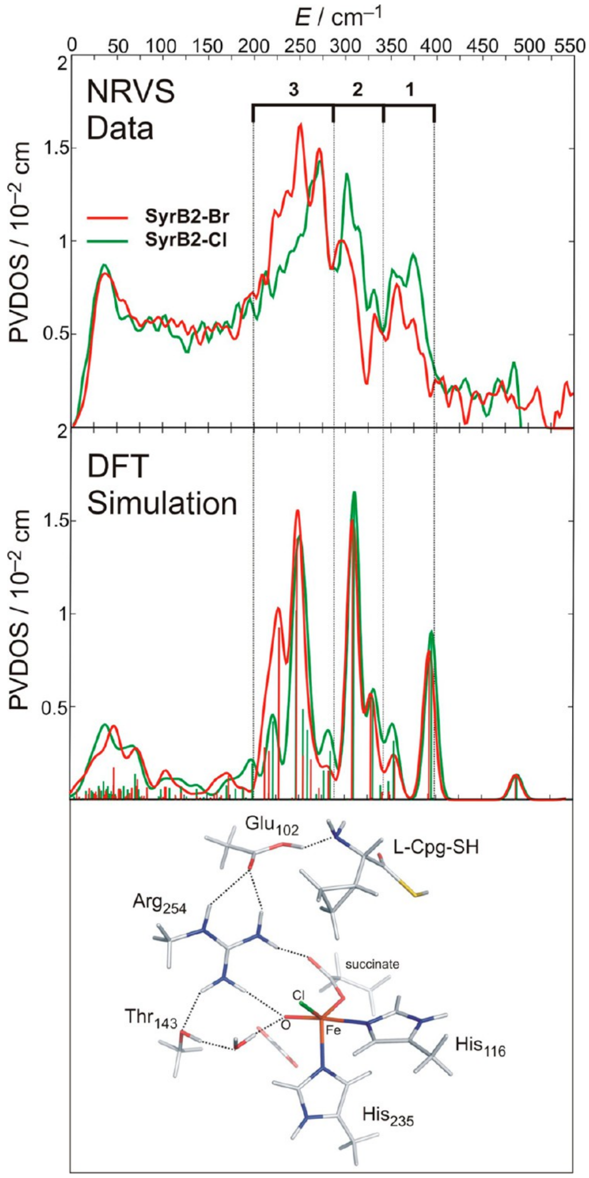

FIGURE 20. Experimental (top) and simulated (middle) NRVS spectra of $Fe^{IV}{=}O$ intermediate of SyrB2, ligated at $Fe^{IV}{=}O$ active site by either Cl^- (green) or Br^- (red). Simulated spectra based on TBP structure with inert substrate L-Cpg (bottom). Adapted from Reference 24.

For correlation to these data, a reaction coordinate was evaluated for SyrB2 using a computational approach calibrated by spectroscopic studies[25] on the stable $\{FeNO\}^7$ analog of the unobserved $\{FeO_2\}^8$ intermediate in HPP-bound HPPD (*vide supra*). (Figure 21, top right) This is a 5C TBP structure consistent with the NRVS data (Figure 20),

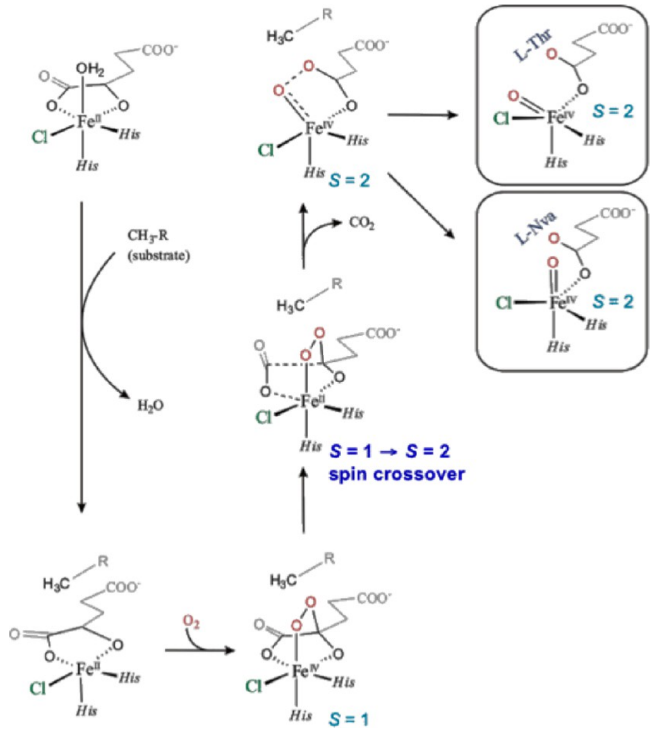

FIGURE 21. O_2 activation in SyrB2 leading to two $Fe^{IV}{=}O$ intermediate orientations relative to substrate (right): perpendicular (native L-Thr) and parallel (non-native L-Nva). Adapted from Reference 24.

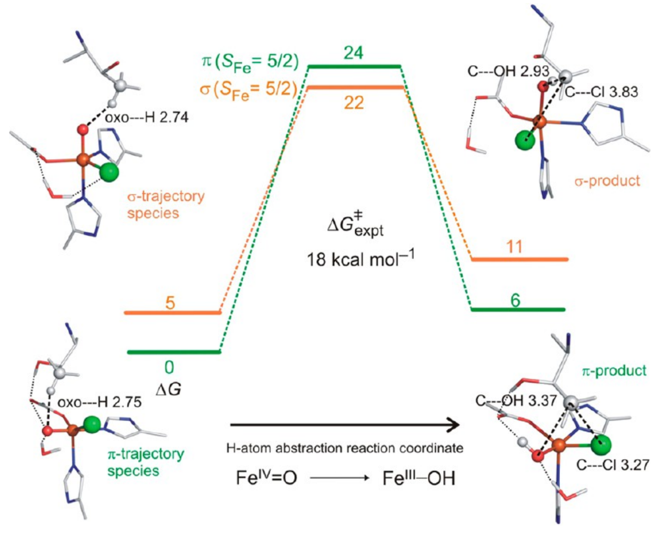

FIGURE 22. SyrB2 H-atom abstraction reaction coordinates for π-trajectory (green) and σ-trajectory (orange). Adapted from Reference 24.

with its Fe–O axis oriented perpendicular to the H–C bond of the native substrate. This structure was used to evaluate the H-atom abstraction reaction. The perpendicular orientation leads to a π-attack on the substrate and produces the H-atom abstracted first product with the halide well-oriented for efficient rebound and the hydroxide ligand oriented away from the radical and stabilized by several hydrogen bonds (Figure 22, green).

In parallel, the O_2 reaction coordinate in Figure 21 was evaluated with the alternative substrate L-Nva, where the difference in substrate hydrogen bonding to the peroxy species generated along the reaction coordinate can lead to an $Fe^{IV}{=}O$ intermediate with its Fe–O axis oriented toward the H–C group of the substrate.[24] The reaction coordinate with this orientation (Figure 22, orange) involves a σ attack on the H–C bond of the substrate with a comparable barrier to the native substrate. This produces a first product with the halide oriented away from the C radical but with the coordinated hydroxide group well-oriented for efficient rebound to form the hydroxylated product as observed (Figure 22).

As shown by our studies on the HPP-dependent enzymes and the halogenases, the $S = 2$ $Fe^{IV}{=}O$ intermediate provides both π and σ FMOs. These have different orientation dependencies, providing an active site flexibility in using this orientation to control reactivity.

5. Concluding Comments

Crystallography, combined with enzymology, synthesis, and kinetics, has revealed important structural types of NHFe enzymes and their reactivities. These are often used as the bases for electronic structure calculations to elucidate mechanism. Here we have emphasized that experimental spectroscopy is key to bridging structure and reactivity with mechanism.

This research is funded by the National Institutes of Health (Grant GM 40392).

BIOGRAPHICAL INFORMATION

Ed Solomon received his Ph.D. from Princeton (with D. S. McClure) and postdoctoral education at the H.C. Ørsted Institute (with C. J. Ballhausen) and at Caltech (with H. B. Gray). He started his career at MIT in 1975 and moved to Stanford in 1982 where he is the Monroe E. Spaght Professor of Humanities and Sciences.

Kenneth Light received a B.S. and M.S. in chemistry from the Colorado School of Mines and is a Ph.D. student at Stanford University. His research focus has included Fe^{II} enzyme control of active site coordination and its contribution to reactivity.

Lei Liu received his B.S. in chemistry from Beijing Normal University and M.S. in chemistry from the University of British Columbia. Lei recently received his Ph.D. from Stanford Univirsity where he focused on peroxo-level intermediates in iron enzymes and models.

Martin Srnec received his Ph.D. from Charles University in Prague and is a postdoctoral fellow at Stanford University. His major interest is in metalloenzymatic reaction mechanisms.

Shaun Wong received his B.S. in chemistry from UC Berkeley and his Ph.D. from Stanford University. His work centered on elucidating the electronic structures and reaction mechanisms of low- and high-spin Fe(IV)−oxo species in enzymes and model complexes.

FOOTNOTES

*Contact information: e-mail edward.solomon@stanford.edu, phone 650-723-9104, fax 650-725-0259.

The authors declare no competing financial interest.

REFERENCES

1 Solomon, E. I.; Brunold, T. C.; Davis, M. I.; Kemsley, J. N.; Lee, S.-K.; Lehnert, N.; Neese, F.; Skulan, A. J.; Yang, Y.-S.; Zhou, J. Geometric and electronic structure/function correlations in non-heme iron enzymes. *Chem. Rev.* **2000**, *100*, 235–349.

2 Que, L., Jr.; Ho, R. Y. N. Dioxygen activation by enzymes with mononuclear non-heme iron active sites. *Chem. Rev.* **1996**, *96*, 2607–2624.

3 Krebs, C.; Galonić Fujimori, D.; Walsh, C. T.; Bollinger, J. M. Non-heme Fe(IV)-oxo intermediates. *Acc. Chem. Res.* **2007**, *40*, 484–492.

4 Kovaleva, E. G.; Niebergall, M. B.; Chakrabarty, S.; Lipscomb, J. D. Finding intermediates in the O_2 activation pathways of non-heme iron oxygenases. *Acc. Chem. Res.* **2007**, *40*, 475–483.

5 Brown, C. D.; Neidig, M. L.; Lipscomb, J. D.; Solomon, E. I. VTVH-MCD and DFT studies of thiolate bonding to $\{FeNO\}^7/\{FeO_2\}^8$ complexes of isopenicillin N synthase: substrate determination of oxidase versus oxygenase activity in nonheme Fe enzymes. *J. Am. Chem. Soc.* **2007**, *129*, 7427–7438.

6 Sono, M.; Roach, M. P.; Coulter, E. D.; Dawson, J. H. Heme-containing oxygenases. *Chem. Rev.* **1996**, *96*, 2841–2888.

7 Pau, M. Y. M.; Lipscomb, J. D.; Solomon, E. I. Substrate activation for O_2 reactions by oxidized metal centers in biology. *Proc. Natl. Acad. Sci. U.S.A.* **2007**, *104*, 18355–18362.

8 Kemsley, J. N.; Mitić, N.; Zaleski, K. L.; Caradonna, J. P.; Solomon, E. I. Circular dichroism and magnetic circular dichroism spectroscopy of the catalytically competent ferrous active site of phenylalanine hydroxylase and its interaction with pterin cofactor. *J. Am. Chem. Soc.* **1999**, *121*, 1528–1536.

9 Light, K. M.; Hangasky, J. A.; Knapp, M. J.; Solomon, E. I. Spectroscopic studies of the mononuclear nonheme FeII enzyme FIH: Second−sphere contributions to reactivity. *J. Am. Chem. Soc.* **2013**, *135*, 9665–9674.

10 Liu, L. V.; Bell, C. B.; Wong, S. D.; Wilson, S. A.; Kwak, Y.; Chow, M. S.; Zhao, J.; Hodgson, K. O.; Hedman, B.; Solomon, E. I. Definition of the intermediates and mechanism of the anticancer drug bleomycin using nuclear resonance vibrational spectroscopy and related methods. *Proc. Natl. Acad. Sci. U.S.A.* **2010**, *107*, 22419–22424.

11 Burger, R. M.; Peisach, J.; Horwitz, S. B. Activated bleomycin - a transient complex of drug, iron, and oxygen that degrades DNA. *J. Biol. Chem.* **1981**, *256*, 1636–1644.

12 Neese, F.; Zaleski, J. M.; Zaleski, K. L.; Solomon, E. I. Electronic structure of activated bleomycin: Oxygen intermediates in heme versus non-heme iron. *J. Am. Chem. Soc.* **2000**, *122*, 11703–11724.

13 Kumar, D.; Hirao, H.; Shaik, S.; Kozlowski, P. M. Proton-shuffle mechanism of O−O activation for formation of a high-valent oxo−iron species of bleomycin. *J. Am. Chem. Soc.* **2006**, *128*, 16148–16158.

14 Chow, M. S.; Liu, L. V.; Solomon, E. I. Further insights into the mechanism of the reaction of activated bleomycin with DNA. *Proc. Natl Acad. Sci. USA* **2008**, *105*, 13241–13245.

15 Decker, A.; Chow, M. S.; Kemsley, J. N.; Lehnert, N.; Solomon, E. I. Direct hydrogen-atom abstraction by activated bleomycin: An experimental and computational study. *J. Am. Chem. Soc.* **2006**, *128*, 4719–4733.

16 Liu, L. V.; Hong, S.; Cho, J.; Nam, W.; Solomon, E. I. Comparison of high-spin and low-spin nonheme FeIII−OOH complexes in O−O bond homolysis and H-atom abstraction reactivities. *J. Am. Chem. Soc.* **2013**, *135*, 3286–3299.

17 Lehnert, N.; Ho, R. Y. N.; Que, L., Jr.; Solomon, E. I. Electronic structure of high-spin iron(III)-alkylperoxo complexes and its relation to low-spin analogues: Reaction coordinate of O-O bond homolysis. *J. Am. Chem. Soc.* **2001**, *123*, 12802–12816.

18 Rohde, J.-U.; In, J.-H.; Lim, M. H.; Brennessel, W. W.; Bukowski, M. R.; Stubna, A.; Münck, E.; Nam, W.; Que, L., Jr. Crystallographic and spectroscopic characterization of a nonheme Fe(IV)═O complex. *Science* **2003**, *299*, 1037–1039.

19 England, J.; Guo, Y.; Farquhar, E. R.; Young, V. G., Jr.; Münck, E.; Que, L., Jr. The crystal structure of a high-spin oxoiron(IV) complex and characterization of its self-decay pathway. *J. Am. Chem. Soc.* **2010**, *132*, 8635–8644.

20 Decker, A.; Rohde, J.-U.; Klinker, E. J.; Wong, S. D.; Que, L., Jr.; Solomon, E. I. Spectroscopic and quantum chemical studies on low-spin Fe^{IV}═O complexes: Fe—O bonding and its contributions to reactivity. *J. Am. Chem. Soc.* **2007**, *129*, 15983–15996.

21 Srnec, M.; Wong, S. D.; England, J.; Que, L., Jr.; Solomon, E. I. π-Frontier molecular orbitals in $S = 2$ ferryl species and elucidation of their contributions to reactivity. *Proc. Natl. Acad. Sci. U.S.A.* **2012**, *109*, 14326–14331.

22 Neidig, M. L.; Decker, A.; Choroba, O. W.; Huang, F.; Kavana, M.; Moran, G. R.; Spencer, J. B.; Solomon, E. I. Spectroscopic and electronic structure studies of aromatic electrophilic attack and hydrogen-atom abstraction by non-heme iron enzymes. *Proc. Natl. Acad. Sci. U.S.A.* **2006**, *103*, 12966–12973.

23 Matthews, M. L.; Neumann, C. S.; Miles, L. A.; Grove, T. L.; Booker, S. J.; Krebs, C.; Walsh, C. T.; Bollinger, J. M. Substrate positioning controls the partition between halogenation and hydroxylation in the aliphatic halogenase, SyrB2. *Proc. Natl. Acad. Sci. U.S.A.* **2009**, *106*, 17723–17728.

24 Wong, S. D.; Srnec, M.; Matthews, M. L.; Liu, L. V.; Kwak, Y.; Park, K.; Bell, C. B.; Alp, E. E.; Zhao, J.; Yoda, Y.; Kitao, S.; Seto, M.; Krebs, C.; Bollinger, J. M.; Solomon, E. I. Elucidation of the iron(IV)−oxo intermediate in the non-haem iron halogenase SyrB2. *Nature.* **2013**, *499*, 320–323.

25 Diebold, A. R.; Brown-Marshall, C. D.; Neidig, M. L.; Brownlee, J. M.; Moran, G. R.; Solomon, E. I. Activation of α-keto acid-dependent dioxygenases: Application of an $\{FeNO\}^7/\{FeO_2\}^8$ methodology for characterizing the initial steps of O_2 activation. *J. Am. Chem. Soc.* **2011**, *133*, 18148–18160.